Supplementary information:
The top-down design of high-performance V-based MBene anode for the Li/Na-ion batteries

Shaohan Li[1], Weiwei Sun[2,3 #*], Tingwei Zhu[4], Siwei Wang[1], Jing Zhang[4*], Jin Yu[1*], Wei Zheng[1], Guobing Ying[1], Litao Sun[4], Huayun Geng[5]

1. School of Materials Science and Engineering, Southeast University, Nanjing, 211189, China
2. Key Laboratory of Quantum Materials and Devices of Ministry of Education, School of Physics, Southeast University, Nanjing, 211189, China
3. Guangxi Key Laboratory of Nuclear Physics and Nuclear Technology, Guilin, 541004, China
4. SEU-FEI Nano-Pico Center, Key Laboratory of MEMS of Ministry of Education, Southeast University, Nanjing, 210096, China
5. National Key Laboratory for Shock Wave and Detonation Physics Research, Institute of Fluid Physics, CAEP, Mianyang, 621900, China

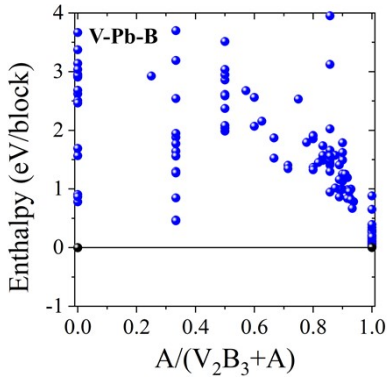

Fig. S1 The binary variable-composition search for V-Pb-B system with respect to V_2B_3 and A phases.

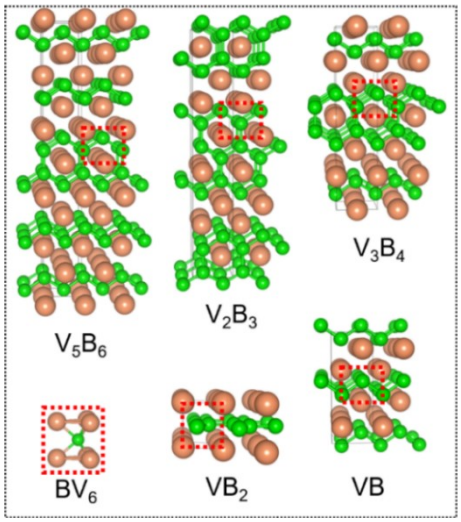

Fig. S2 Crystal structures of layered V_xB_z compounds (V_5B_6, V_2B_3, VB_2, V_3B_4, and VB). BV_6 unit is framed in the red dotted box.

Since hex-V_4PB_6 has thicker M_xB_z layers, its out-of-plane lattice constant *c* (12.244 Å) is larger than

that of Ti_2InB_2 (7.917 Å) and Hf_3InB_4 (11.868 Å), while its in-plane parameter *a* (3.015 Å) keeps the same level with them (3.077 Å and 3.182 Å), as shown in Table S1. Crossing bands at the Fermi energy (E_f) for hex-V_4PB_6 shown in Fig. S4a represent its metallic feature. The hybridization of V_3*d* and P_3*p* orbitals located near -1.5 eV and the hybridization of V_3*d* and B_2*p* orbitals observed in the area lower than -3.4 eV in the density of states (DOS) part of Fig. S4a indicate the V-P bond and stronger V-B bonds. The ELF results in Fig. S4b reveal that there is obvious electron accumulation around P atoms, and significant sharing electron density between adjacent boron atoms means the covalent B-B bonds inside the boron sheet.

Table S1 Crystallographic structure information of hex-V_4PB_6 ($P\bar{6}m2$, No. 187) and orth-V_4PB_6 (*Cmmm*, No. 65).

Phases	Space group	Energy (eV/atom)	Lattice constants (Å)			Atom sites		
			a	*b*	*c*	Atom	Position	Coordinate
V_4PB_6	$P\bar{6}m2$	-8.165	3.015	3.015	12.244	V	2*h*	(1/3, 2/3, 0.134) (1/3, 2/3, 0.378)
						P	1*a*	(0, 0, 0)
						B	2*i*	(2/3, 1/3, 0.253)
							2*g*	(0, 0, 0.253)
							1*b*	(0, 0, 0.5)
							1*f*	(2/3, 1/3, 0.5)
V_4PB_6	*Cmmm*	-8.041	2.988	20.956	3.039	V	4*i*	(0.5, 0.431, 0) (0.5, 0.188, 0) (0, 0.069, 0) (0, 0.312, 0)
						P	2*c*	(0.5, 0, 0.5)
						B	4*j*	(0, 0.396, 0.5) (0, 0.146, 0.5) (0, 0.229, 0.5) (0.5, 0.104, 0.5) (0.5, 0.354, 0.5) (0.5, 0.271, 0.5)

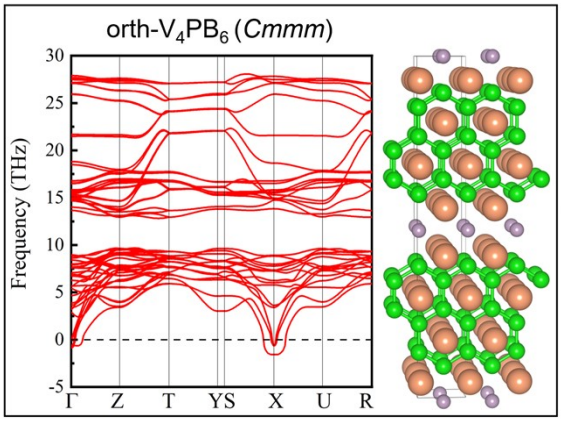

Fig. S3 The phonon dispersion curve and crystal structure for orth-V_4PB_6 (*Cmmm*).

Table S2 Calculated bulk modulus B (GPa), shear modulus G (GPa), Young's modulus E (GPa), Poisson's ratio v and Vickers hardness H_V^{Chen}, H_V^{Tian} (GPa) of hex-V_2PB_2 ($P\bar{6}m2$), hex-V_3PB_4 ($P\bar{6}m2$), hex-V_4PB_6 ($P\bar{6}m2$), binary compound orth-V_2B_3 ($Cmcm$), hex-V_4AlC_3 ($P6_3/mmc$) and orth-Cr_4AlB_6 ($Cmmm$).

Phases	V_2PB_2	V_3PB_4	V_4PB_6	V_2B_3	Cr_4AlB_6	V_4AlC_3
C_{11}	472	545	583	502	455	456
C_{12}	108	109	112	146	136	116
C_{13}	140	139	137	138	138	120
C_{22}	-	-	-	647	572	-
C_{23}	-	-	-	109	139	-
C_{33}	459	474	478	663	516	385
C_{44}	226	232	230	251	191	173
C_{55}	-	-	-	230	154	-
C_{66}	182	232	235	258	192	170
B	242	260	268	287	262	223
G	193	219	222	241	182	165
E	457	513	521	564	443	398
v	0.19	0.17	0.18	0.17	0.22	0.20
H_V^{Chen}	30.22	35.28	34.74	37.16	24.27	25.01
H_V^{Tian}	29.41	34.36	33.95	36.48	24.08	24.39

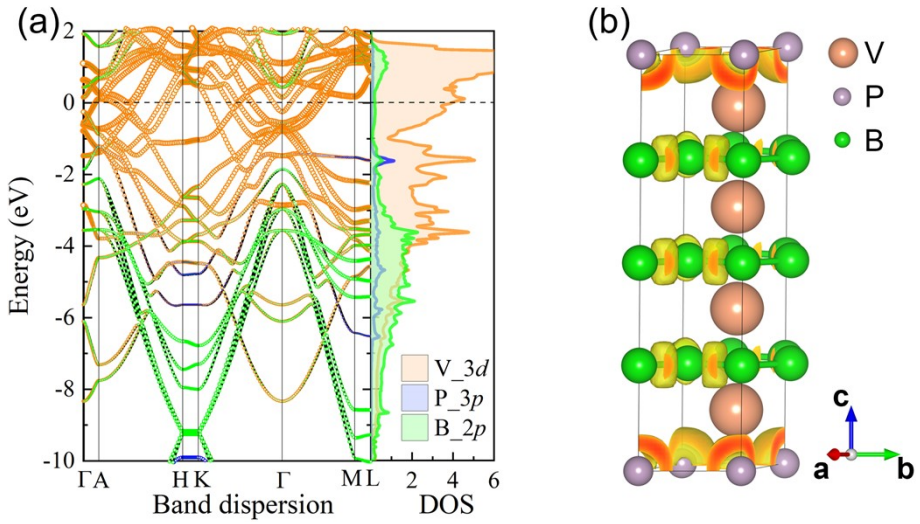

Fig. S4 (a) The projected band structure and density of states (DOS) for hex-V_4PB_6 ($P\bar{6}m2$). The Fermi energy (E_f) is indicated by solid line at 0 eV. In the picture, DOS are measured in the unit of states/eV. (b) The three-dimensional electron localization function (ELF) with a value of isosurface 0.7 for hex-V_4PB_6 ($P\bar{6}m2$).

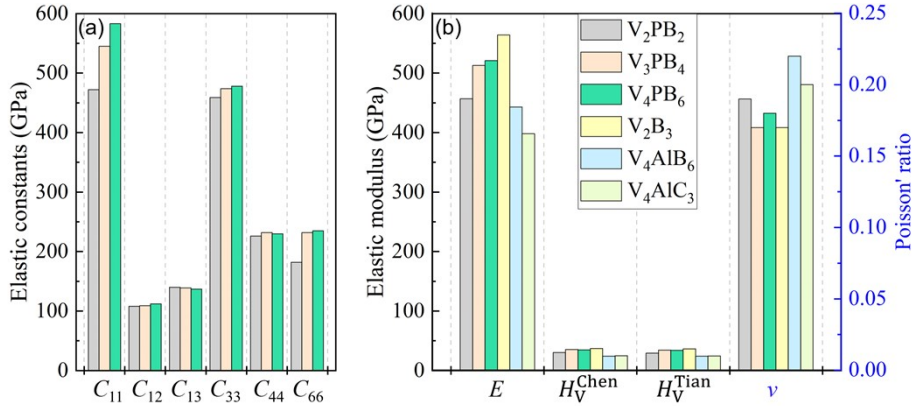

Fig. S5 (a) Calculated elastic constants for hex-V_2PB_2 ($P\bar{6}m2$), hex-V_3PB_4 ($P\bar{6}m2$), hex-V_4PB_6 ($P\bar{6}m2$). (b) Calculated elastic modulus and Poisson's ratio for hex-V_2PB_2 ($P\bar{6}m2$), hex-V_3PB_4 ($P\bar{6}m2$), hex-V_4PB_6 ($P\bar{6}m2$), binary compound orth-V_2B_3 (*Cmcm*), hex-V_4AlC_3 (*P*6$_3$/*mmc*) and orth-Cr_4AlB_6 (*Cmmm*).

For the M-A, M-B and A-A bonds in MAB phases, their interlayer distance at ground state is d_0. As the distance d increases, the energy of compounds becomes higher, and until d is large enough, the energy no longer changes. Taking M-A bond for example, the relative energy can be obtained from the following equation:

$$E_{relative} = -(E_{MAB} - E_{MB-A})/S \quad \text{(S1)}$$

where E_{MAB} is the total energy of ground-state MAB phase, and E_{MB-A} is the total energy of MAB phase with an interlayer distance d between MB and A layers. S represents the in-plane surface area of the unit cell of the MAB phase. The bonding energy of the M-A bond is the convergent value of relative energy.

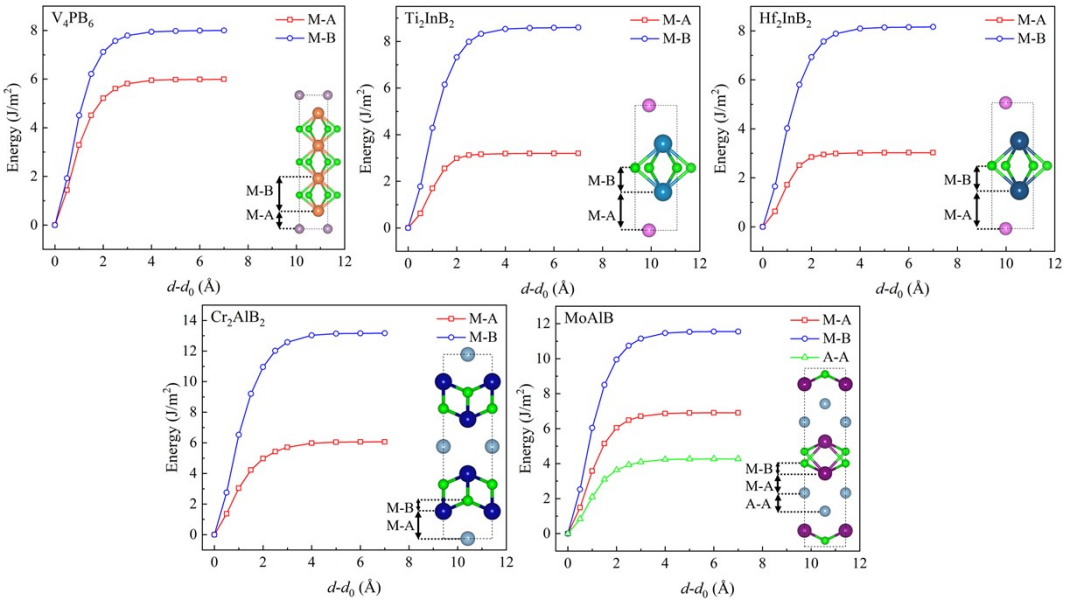

Fig. S6 Calculated energy varying with d-d_0 for hex-V_4PB_6 ($P\bar{6}m2$), hex-Ti_2InB_2 ($P\bar{6}m2$), hex-Hf_2InB_2 ($P\bar{6}m2$), orth-Cr_2AlB_2 (*Cmmm*), and orth-MoAlB (*Cmcm*).

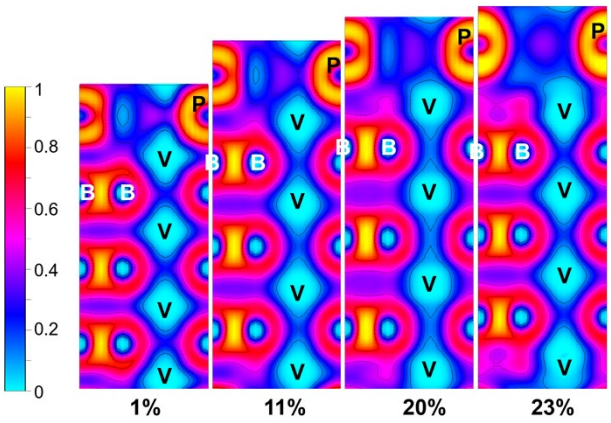

Fig. S7 The electron localization function (ELF) contour plots along the (110) plane for hex-V_4PB_6 ($P\bar{6}m2$) under [001] tensile strains of 1%, 11%, 20% and 23% with an isosurface value 0.85.

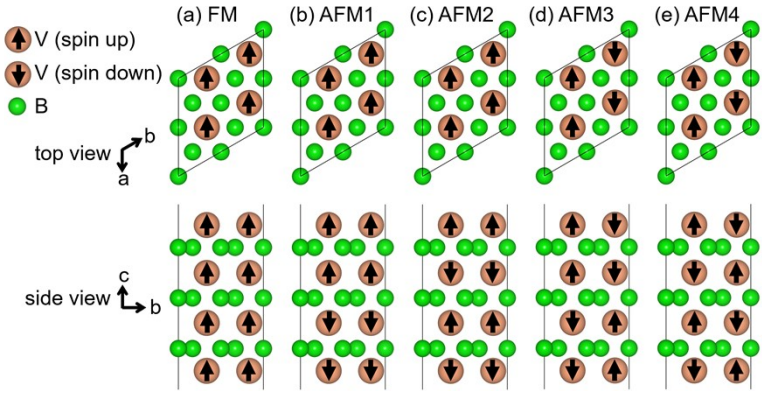

Fig. S8 Diagram of five magnetic configurations using V_4B_6 as an example: (a) ferromagnetic (FM), and antiferromagnetic (AFM) including (b) AFM1, (c) AFM2, (d) AFM3, (e) AFM4.

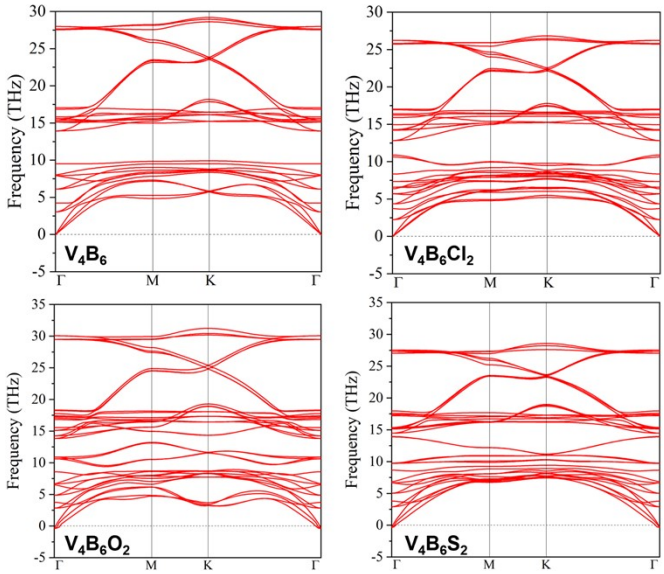

Fig. S9 Calculated phonon dispersion spectra of 2D V_4B_6 and $V_4B_6T_2$ (T = Cl, O, and S).

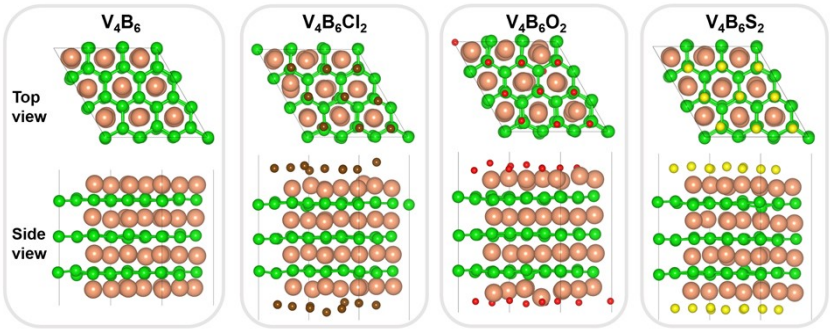

Fig. S10 Top and side views of equilibrium structures for 2D V_4B_6 and $V_4B_6T_2$ (T = Cl, O, and S) after undergoing a 5 ps AIMD simulation at 900 K.

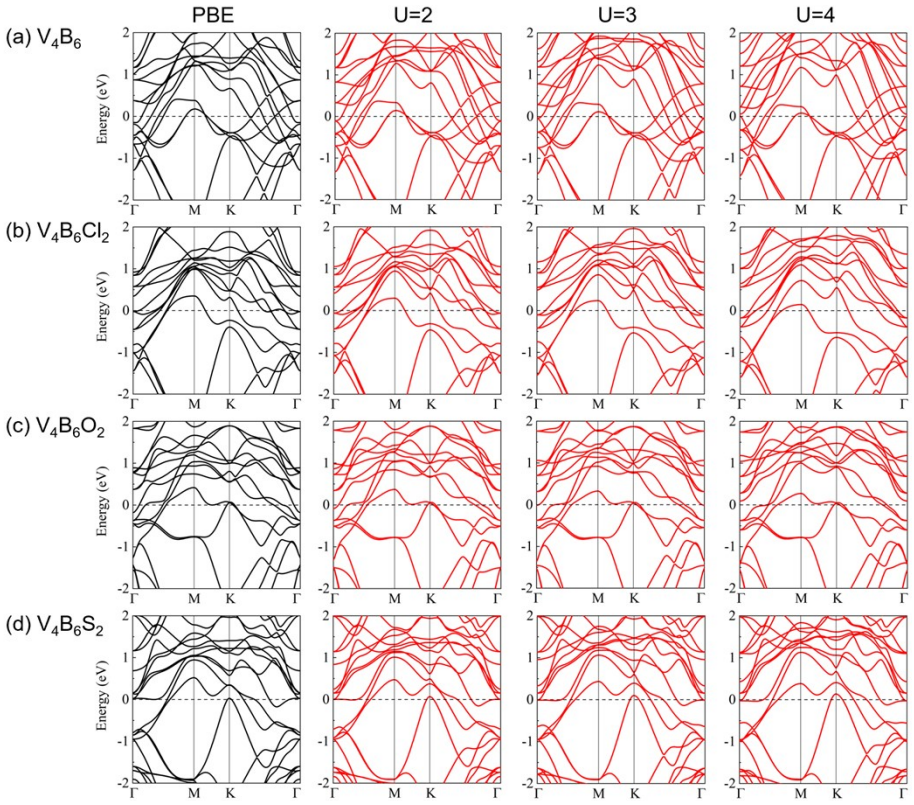

Fig. S11 Calculated band structures using PBE and PBE+U with U = 2 eV, 3 eV, 4 eV for (a) V_4B_6, (b) $V_4B_6Cl_2$, (c) $V_4B_6O_2$, and (d) $V_4B_6S_2$.

Table S3 The space group, lattice constants a, and elastic constants (C_{ij}) of 2D V_4B_6, $V_4B_6Cl_2$, $V_4B_6O_2$, and $V_4B_6S_2$.

	V_4B_6	$V_4B_6Cl_2$	$V_4B_6O_2$	$V_4B_6S_2$
Space group	$P6/mmm$	$P\bar{6}m2$	$P\bar{3}m1$	$P\bar{6}m2$
a (Å)	2.976	3.030	2.936	3.011
C_{11} (N/m)	640	650	733	721
C_{12} (N/m)	82	96	128	116
C_{66} (N/m)	279	277	303	302

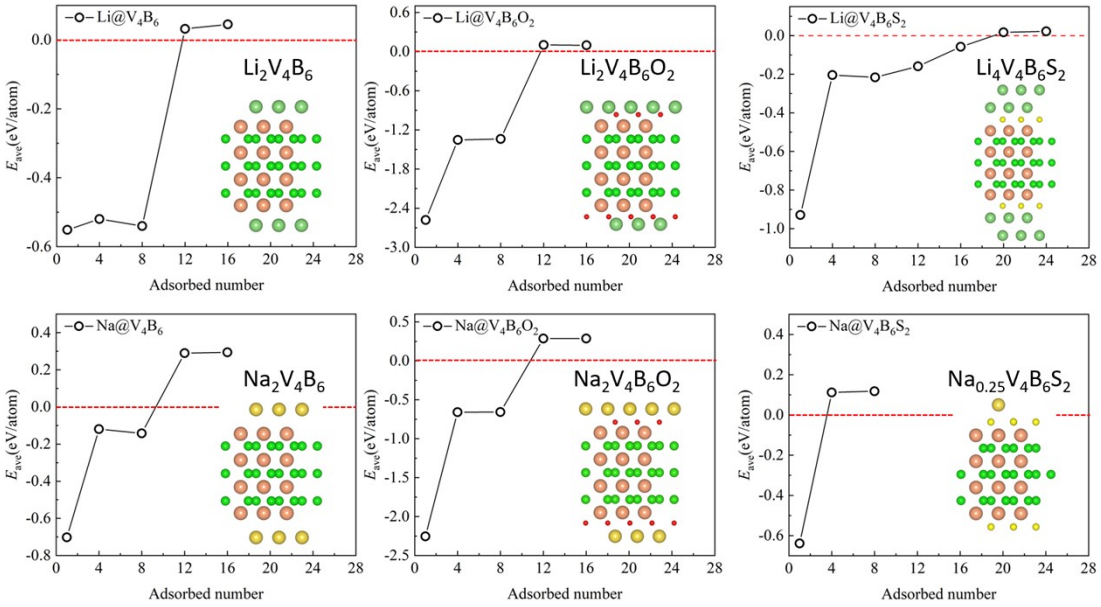

Fig. S12 The average adsorption energy (E_{ave}) with increasing adsorbed Li/Na layers on 2D V_4B_6, $V_4B_6Cl_2$, $V_4B_6O_2$ and $V_4B_6S_2$ monolayers. The inset is the side view of structures of $Li_2V_4B_6$, $Li_{0.25}V_4B_6Cl_2$, $Li_2V_4B_6O_2$, $Na_2V_4B_6$, $Na_2V_4B_6O_2$ and $Na_{0.25}V_4B_6S_2$ with the largest number of Li/Na layer.

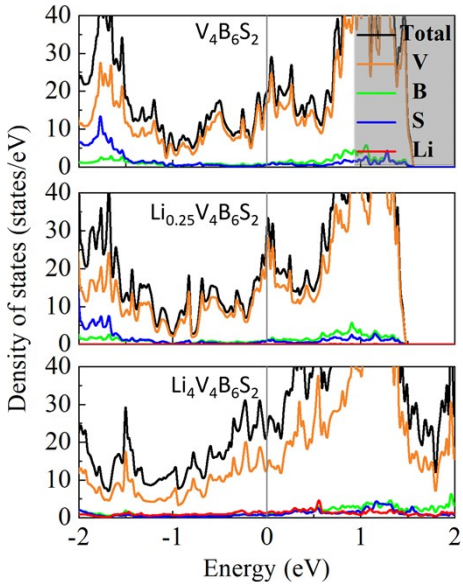

Fig. S13 The elementary density of states (DOS) of the $V_4B_6S_2$, $Li_{0.25}V_4B_6S_2$, and $Li_4V_4B_6S_2$.

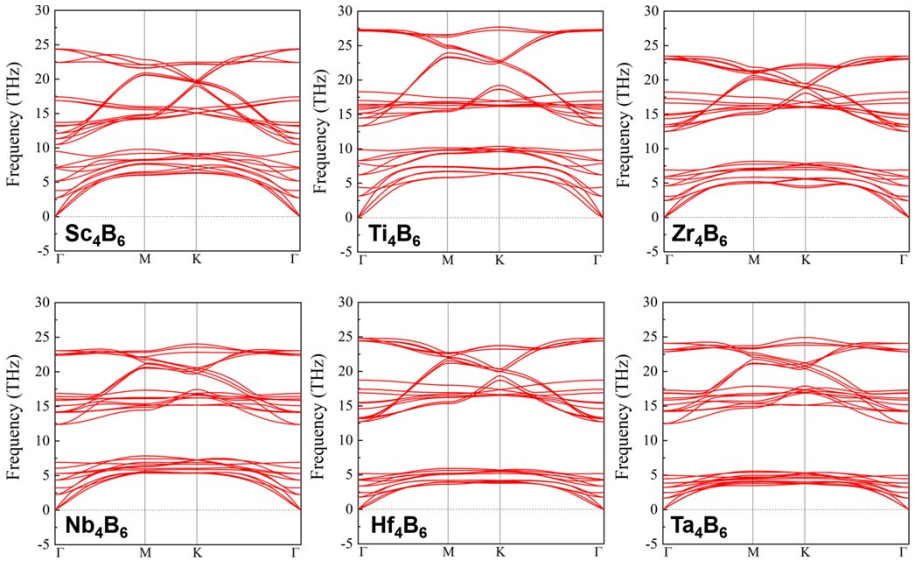

Fig. S14 Calculated phonon dispersion spectra of 2D h-M_4B_6 (M = Sc, Ti, Zr, Nb, Hf, and Ta).

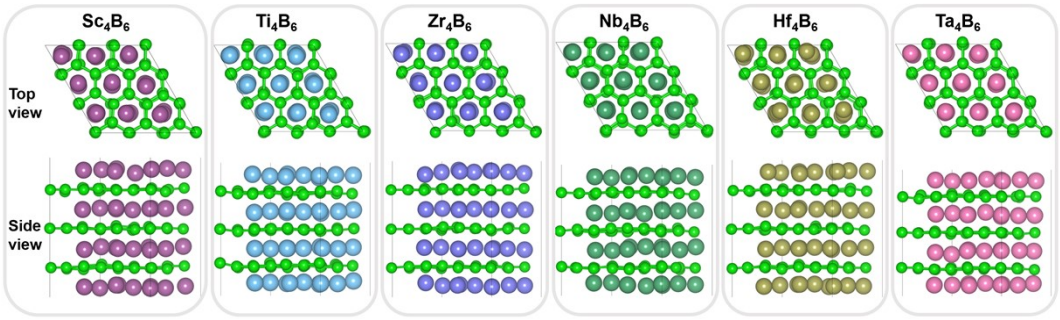

Fig. S15 Top and side views of equilibrium structures for 2D h-M_4B_6 (M = Sc, Ti, Zr, Nb, Hf, and Ta) after undergoing a 5 ps AIMD simulation at 900 K.